Applied Catalysis B: Environmental 237 (2018) 791–801

Contents lists available at ScienceDirect

Applied Catalysis B: Environmental

journal homepage: www.elsevier.com/locate/apcatb

Anchoring MWCNTs to 3D honeycomb ZnO/GaN heterostructures to enhancing photoelectrochemical water oxidation

Santosh S. Patil[a], Muhammad Ali Johar[a], Mostafa Afifi Hassan[a], Deepak R. Patil[b], Sang-Wan Ryu[a,*]

[a] Department of Physics, Chonnam National University, Gwangju, 61186, Republic of Korea
[b] Centre for Materials for Electronics Technology (C-MET), Department of Electronics and Information Technology (DeitY), Govt. of India, Pune, 411008, India

ARTICLE INFO

Keywords:
Ternary heterostructure
GaN/ZnO/MWCNTs
Hydrothermal
Nanoflakes
Photoelectrochemical water oxidation

ABSTRACT

Gallium nitride (GaN) is one of the ubiquitously known photoanode for photoelectrochemical water splitting (PEC-WS) due to its tunable band gap and favorable band edge positions. However, the unavoidable surface defects in GaN induces surface Fermi level pinning and surface band bending which severely reduces its PEC conversion efficiency. Constructing heterostructure is the key to approaching better charge separation efficiency and light harvesting ability for PEC-WS. Considering this, we have fabricated ternary heterostructure of GaN/ZnO/MWCNTs photoanode by combining metal organic chemical vapour deposition (MOCVD), hydrothermal and 'dip and dry' methods. FE-SEM results showed the formation of 3D hierarchical honeycomb structure of ZnO on GaN thin film surface when MWCNTs are added into hydrothermal reaction. We investigate the advantage of ZnO honeycomb structure in enhancing the solar PEC-WS performance of GaN photoanode. The synergy of incorporating MWCNTs has resulted into improvement in surface morphology, electron transportation and light harvesting capability. The as obtained ternary heterostructure exhibits photocurrent (J_{ph}) of 3.02 mA/cm^2 at 0 V versus Pt electrode under 1-sun light illumination which is about 2.58 times higher than that of pristine GaN photoanodes (J_{ph} = 1.14 mA/cm^2).

1. Introduction

Photoelectrochemical water splitting (PEC-WS) promises an attractive route for solar energy conversion and storage [1]. Increasing solar-to-hydrogen conversion efficiency (STH%) > 15% is one of the key challenges towards large scale utilization of PEC-WS devices [2,3]. The insufficient STH% of current devices is mainly due to unavailability of robust and high-efficiency photoelectrode materials [3,4]· Metal oxides have been most studied photoanodes for PEC-WS due to their robustness in aqueous electrolytes, low cost and environmental sustainability [3,5]. However, most of them possess wide bandgaps which limit their use to effectively harvest a wide range of solar spectrum. Moreover, they are succumbed to rapid recombination of photo-induced charge carriers (e^-/h^+) which is very critical to achieve high efficiency from photoelectrodes [6]. To overcome these limitations researchers have adopted the concept of heterostructure construction strategy by combining two or more semiconductors or metals, which indeed yield improved sunlight absorption, electron–hole (e^-/h^+) pair separation, carrier collection and high photoconversion efficiencies [7,8]. For example, heterostructures including $TiO_2/BiVO_4$ [9], TiO_2/MWCNTs [10], $SrTiO_3/TiO_2$ [11], GaN/InGaN [12], MoS_2/CdS [13], SnO_2@MoS_2 [14], SnO_2/ZnO [15], α-Fe_2O_3/Graphene/$BiV_{1-x}Mo_xO_4$ [16], ZnO/CuO [17], ZnO/Ag [4] and others have shown significant enhancement in the PEC-WS efficiency compared to their individual counterparts. Several theoretical studies have also been undertaken to find ideal combination of different materials for heterostructure construction. Gallium nitride/Zinc oxide heterostructure is one of the best pairs for PEC-WS; however their photocurrent densities are insufficient [18]. GaN and ZnO are highly complementary for each other, because they possess the same wurtizite crystal structure and lower lattice mismatch (1.8%), which make them suitable candidates to form a heterostructured photocatalyst for PEC-WS devices [6,18]. However, the growth of nanoscale ZnO with high crystal quality and high aspect ratio is quite challenging.

Previously, GaN/ZnO composites have also been tested as photocatalyst for water splitting, wherein GaN:ZnO photoanodes were generally fabricated by coating as-synthesized GaN:ZnO particles onto a conductive substrate using physical methods. However, in these photoanodes, the connection between the adjacent GaN:ZnO particles and the adhesion between GaN:ZnO film and conductive substrate are poor,

* Corresponding author.
E-mail address: sangwan@chonnam.ac.kr (S.-W. Ryu).

https://doi.org/10.1016/j.apcatb.2018.06.047
Received 29 December 2017; Received in revised form 7 June 2018; Accepted 17 June 2018
Available online 19 June 2018

which inevitably retards the interfacial charge transfer and leads to charge recombination [19]. Alternatively, the direct deposition of ZnO nanostructures onto GaN substrate to form a GaN/ZnO heterostructure photoanode could be a very promising approach, because it offers strong interaction and good adhesion for efficient charge separation across interface. Additionally, combining these heterostructures with carbon nanotubes (CNT) or multiwalled carbon nanotubes (MWCNTs) endows composite effect with unique properties in heterogeneous catalysis [20–22]. Interestingly, most recent works have suggested that the morphology, structure, composition and catalytic activity of metal oxides could be greatly influenced by introducing MWCNTs [20,22]. For instance, Li et al. [21] have fabricated CoMnAl-layer double oxides in the absence and presence of MWCNTs using homogeneous urea precipitation method showing drastic change in surface morphology from regular 2D-hexagonal plate-like structure to 3D hierarchical honeycomb structure resulting in high catalytic activity for organic bisphenol degradation. Likewise, Dang et al. [21] prepared hollow MnO_2 nanotubes with highly porous walls under the influence of MWCNTs and found that superior performance for photocatalytic organic dye degradation. Additionally, MWCNTs have been used as a promising promoter material in the field of photocatalytic water splitting, owing to their high electrical and thermal conductivities and large surface area [23].

Herein, we have demonstrated the synthesis of ternary heterostructure GaN/ZnO/MWCNTs photoanode for PEC-WS. The particular emphasis is placed on investigating the role of MWCNTs on changing the ZnO surface morphology and their correlation with PEC performances. The results signify that the electronic conductivity and charge transportation can be enhanced by integrating MWCNTs into GaN/ZnO heterostructures, as observed by impedance spectroscopy. Similarly, the cathodic shift in onset potential is observed owing to the synergistic effect of heterostructure enabling the enhanced photocurrent density. Although, there are few previous reports on use of GaN/ZnO heterostructures for PEC-WS, their PEC performances are very low as well as research efforts couldn't have focused on unassisted PEC-WS. In this paper, efforts are mainly focused on achieving unassisted water splitting and correlating photoanodes structure with PEC performance. It is noteworthy that, the direct hydrothermal thin film photoanode synthesis is crucial, due to the low-temperature, modest-cost, highly scalable, and relatively simple fabrication procedure, and therefore can be employed for developing unique 3D hierarchical nanostructures for PEC-WS applications.

2. Experimental

2.1. Preparation of GaN thin film

All the chemicals were of analytical grade and used without further purification. The GaN thin film was prepared on (0001) sapphire substrate using metal-organic chemical vapour deposition (MOCVD). The as-prepared GaN thin film was labeled as GZ0. In a typical synthesis of GaN thin film, trimethylgallium (TMGa) and ammonia (NH_3) were used as sources of gallium and nitrogen, respectively. In order to decrease the defect density in the GaN thin film, a low-temperature buffer layer was grown at 600 °C for 130 s, with TMGa and NH_3 flow rates of 118 μmol min^{-1} and 267 mmol min^{-1}, respectively. Then reactor temperature was increased to 1175 °C and the flow rates of TMGa and NH_3 were increased to 293 μmol min^{-1} and 424 mmol min^{-1}, respectively, with a V/III ratio of 1450. The growth time and reactor pressure were 5500 s and 200 torr, respectively. Finally, the reactor was allowed to cool down in a nitrogen atmosphere until the temperature reached 300 °C. Thus, a 2.5-μm-thick *c*-axis GaN thin film was successfully grown on a GaN/sapphire substrate. Then the substrates were taken out of the reactor at a temperature of approximately 130 °C and used for further characterizations. Electrical properties of as prepared GaN thin film are summarized in Table S2.

2.2. Synthesis of GaN/ZnO heterostructures

The MOCVD-grown GaN/sapphire substrates were used for the construction of hybrid heterostructure photoelectrodes. The growth of the ZnO nanostructures on GaN/sapphire substrates was carried out using a facile hydrothermal method. In a typical experiment, 0.09 g zinc nitrate hexahydrate ($ZnNO_3.6H_2O$; 98%; DAEJUNG) and 0.09 g hexamethyl tetraamine (HMT; 99%; DAEJUNG) were dissolved into 60 mL distilled water. Then, the solution was magnetically stirred for 15 min. Subsequently, for the growth of the ZnO nanostructures, the GaN/sapphire substrate was placed into a hydrothermal reactor with the GaN thin film facing down at an angle of approximately 45° to the wall of the Teflon vessel. Later, the as-prepared reaction solution was transferred into a Teflon rector and placed into a stainless-steel autoclave. The autoclave was then kept in an oven at 95 °C for 8 h. When the reaction time had elapsed, the autoclave was allowed to cool naturally to room temperature. The substrate was removed, washed with distilled water, and kept in an oven for drying at 60 °C for 2 h. The as-synthesized GaN/ZnO heterostructure sample was labeled as GZ1.

2.3. Functionalization of multiwalled carbon nanotubes

Commercial multiwalled carbon nanotubes (MWCNTs) were purchased from Hanwha Chemical Co Ltd. (Korea) and used for further synthesis. Prior to their use, the as-purchased MWCNTs were functionalized by refluxing them using concentrated H_2SO_4:HNO_3 (3:1) in order to achieve the binding of functional groups (carboxylic and/or hydroxyl) to the walls. The dispersed MWCNTs solution was ultrasonicated for 1 h and refluxed at 80 °C for 4 h. Subsequently, the precipitate was collected by centrifugation, washed thoroughly using distilled water to eliminate the acid, and dried at 70 °C overnight. The as-obtained MWCNTs (0.01 g) were dispersed into 50 mL distilled water and ultrasonicated for 3 h to achieve uniform dispersion of the MWCNTs. This solution was further used as a precursor solution for the synthesis of the GaN/ZnO/MWCNTs heterostructure thin film electrodes.

2.4. Synthesis of GaN/ZnO/MWCNTs heterostructures

The main motivation of the present work is to improve the solar-to-hydrogen conversion efficiency of GaN-based photoanodes for PEC-WS devices. Therefore, we adopted a heterostructure construction strategy by combining GaN with a promising semiconductor (ZnO) and an emerging conducting material (MWCNTs). Facile and inexpensive synthesis methods, such as the hydrothermal and conventional dip-and-dry method, have been investigated to prepare ternary heterostructure GaN/ZnO/MWCNTs thin films. Hierarchical ZnO nanostructures were grown on GaN/sapphire substrates using a facile hydrothermal method (Scheme 1). It was understood that the direct hydrothermal growth of ZnO nanostructures on GaN/sapphire substrates depends on two important parameters: (i) Prior to the reaction, the GaN/sapphire substrate should be immersed and placed into the reactor solution in such a way that the GaN thin film side faces in a downward direction (at an angle of approximately 45°) to the wall of the Teflon vessel to avoid the particle settlement (ii) It should be ensured that there is not an initial formation of the precursor complex (precipitate). If the precipitate is formed before the hydrothermal reaction, it simply gets collected at the bottom of reactor, and no growth or deposition occurs. Therefore, the appropriate selection of the precursors and the reaction conditions play a crucial role in the growth of GaN/ZnO heterostructures. An attempt to effect in-situ integration of the MWCNTs with the GaN/ZnO heterostructure was made. A synthesis procedure similar to that of GZ1 was repeated with the addition of MWCNTs precursor solution (10 mL) to the reaction solution. The C elemental composition was found to approximately 0.76 wt% as revealed from the EDS spectra (Supporting information Table S1, Fig. S5). The hydrothermal growth process was

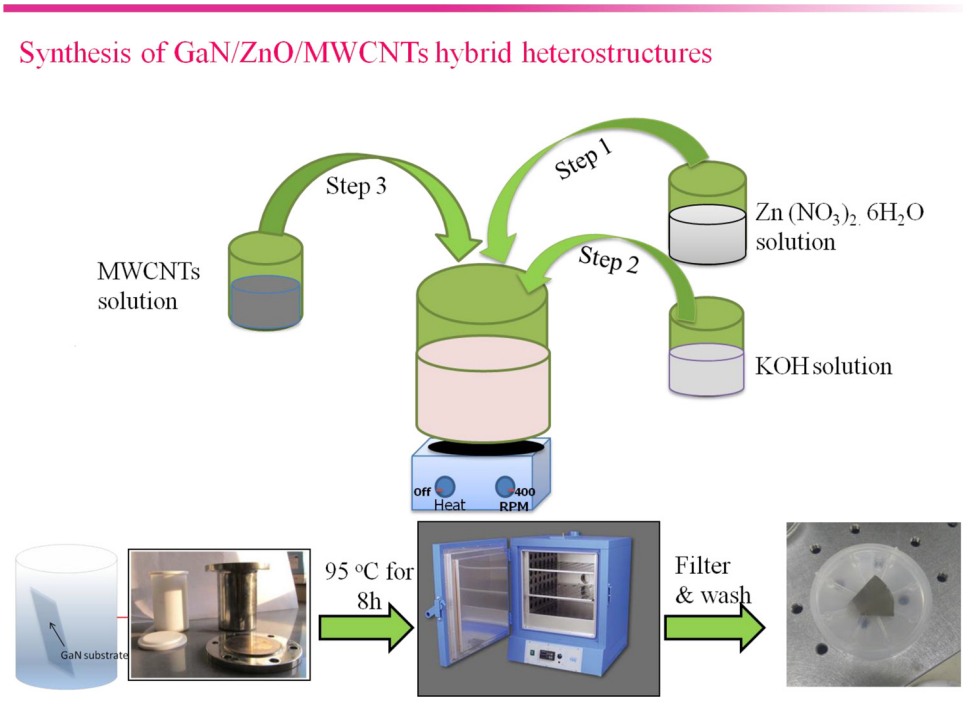

Scheme 1. Schematic representation of hydrothermal synthesis process for GaN/ZnO/MWCNTs hybrid heterostructures.

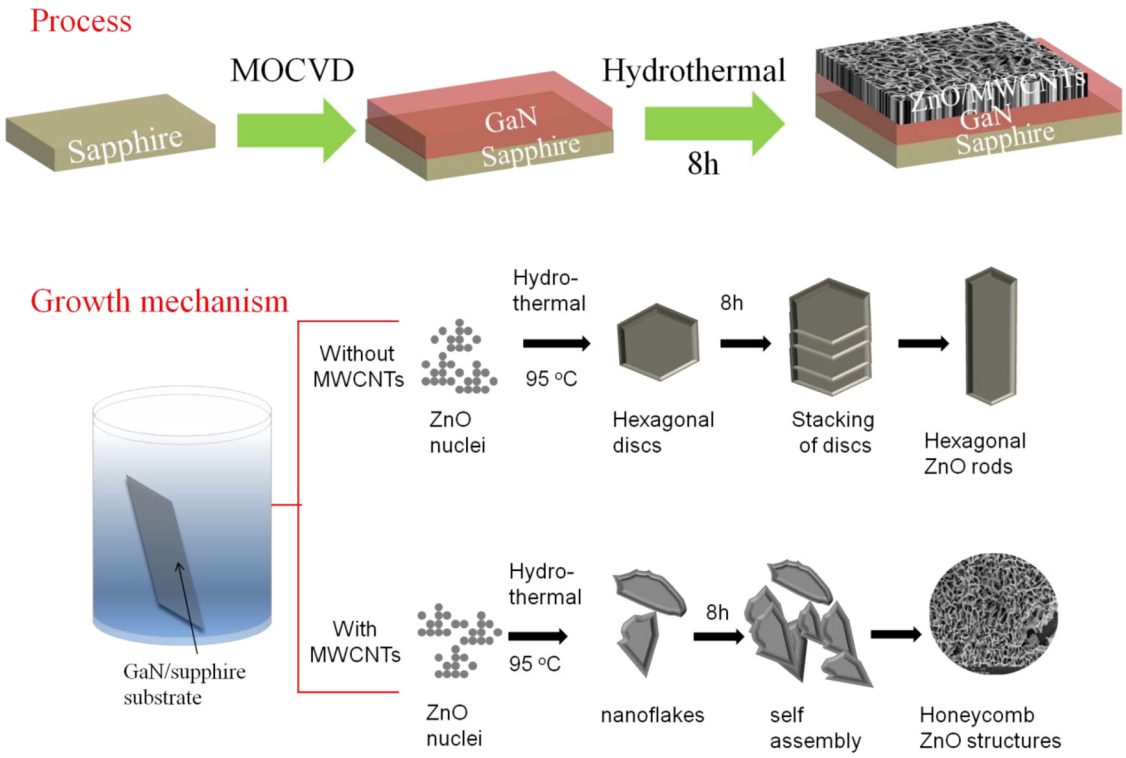

Scheme 2. Schematic showing photoelectrode preparation process and involved growth mechanism.

performed and the sample was then labeled as GZ2. From the preliminary characterizations of GZ2, we did not observe MWCNTs at the surface. Therefore, an attempt was made to use the conventional dip-and-dry method to incorporate MWCNTs into heterostructure thin film. A similar synthesis strategy to that of GZ2 was repeated. The GZ2 sample was prepared, and the further integration of MWCNTs was effected by the dip-and-dry method. In a typical process, we immersed a GZ2 sample into the MWCNTs solution for 30 s, and the electrostatic force of attraction between the substrate and the MWCNTs solution enabled the deposition. Subsequently, the film was taken out and dried using an air-drier, thereby completing one cycle. We repeated this twice in order to obtain good adhesion and uniformity, and the sample was labeled as GZ2-2T (Fig. S1a). The schematic representation of hydrothermal synthesis and preparation process is illustrated in Schemes 1 and 2, respectively.

2.5. Materials characterization

XRD (X'Pert PRO, PANalytical system) was used to determine the phase formation and crystal structure of thin film samples. Raman spectra were obtained using an excitation wavelength 514 nm with a Raman microscope (LabRam HR8000, Horiba Jobin-Yvon). A field-emission scanning electron microscope equipped (FESEM) with an EDS analyzer (S 4800, Hitachi) was used to investigate the surface morphology and elemental composition. The FE-TEM sample was prepared using FIB (FEI, Helios NanoLab G3 CX). HRTEM (JEOL-3010) with an operating voltage of 300 kV was used to observe the microstructure. The elemental surface composition of the thin film samples was investigated using High-resolution XPS (HR-XPS, VG Multi lab 2000, Thermo VG Scientific). Cyclic voltametry (CV) was performed using potentiostat (PARSTAT 3000) with a standard three cell system which comprised of working electrodes of GZ0, GZ1, GZ2 and GZ2-2T samples, a platinum counter electrode, and an SCE reference electrode in 1 M NaOH. The optical absorption spectra were measured by using a UV–vis spectrometer (Lambda 950 spectrometer, Perkin-Elmer). Photoluminescence (PL) spectra were recorded by using intensified CCD (P1-Max3) (Princeton Instrument) with a diode pumped solid state laser (Ekspla) with an excitation wavelength of 266 nm.

2.6. Photoelectrochemical (PEC) water splitting

To evaluate the water splitting properties of the as-prepared thin film samples, a homemade PEC cell composed of a Teflon chamber was used (Fig. S1b). A PEC cell with a two-electrode configuration connected to a high-polarization potentiostat (PARSTAT 3000) was used and the PEC-WS characteristics were investigated using a 0.5 M NaOH (pH-13) aqueous electrolyte. The as-prepared GaN/ZnO/MWCNTs (GZ series) thin film samples were used as the photoelectrode, whereas a Pt wire serves as the counter electrode. The photoelectrodes with exposed O-ring surface area (approximately 0.52 cm^2) were kept in direct contact with the electrolyte and mounted on the Teflon chamber. A quartz window was set up to pass light to the Teflon chamber from a Xe lamp (300 W) with a light intensity of approximately 100 mW/cm^2. Furthermore, to measure the incident photon to current conversion efficiency (IPCE), bandpass filters with different passbands were used.

3. Results and discussion

Fig.1a and b depicts surface morphological features of as prepared heterostructure GaN/ZnO thin film (GZ1). The formation of hexagonal rods with approximate length 0.5–1 μm and diameter ~100 nm were observed. It is interesting to note that the surface morphology of ZnO was dramatically changed from hexagonal nanorods/discs to 3D hierarchical honeycomb after introduction of MWCNTs into the hydrothermal reaction. Fig. 1c and d displays the FESEM micrographs of hydrothermally prepared GaN/ZnO heterostructures with addition of MWCNTs (GZ2 photoelectrode). The special porous 3D hierarchical honeycomb ZnO structures are confirmed which is formed by interconnected nanosheets arrays having average diameter of ~30–40 nm and length of ~300–500 nm. Such unique porous hierarchical 3D honeycomb structures have attracted expectant research attention due to their interconnected network and large surface area, which is quite advantageous for better semiconductor/electrolyte contact and facile charge transportation in PEC devices [24–26].

During the hydrothermal reaction, the hydration of the precursors (zinc nitrate hexahydrate and HMT) takes place, which provides the Zn cations and hydroxide anions that further react to form stable Zn $(OH)_4^{2-}$ complexes. The as-formed $Zn(OH)_4^{2-}$ complexes act as growth units of the ZnO nanostructures. It is worth noting that the Zn $(OH)_4^{2-}$ anions are generated at a slower rate, because HMT generates hydroxide anions slowly as compared to ammonia–water. Therefore, HMT has been widely used as a precursor for the growth of hierarchical ZnO nanostructures. The chemical reaction can be expressed as,

$$C_6H_{12}N_4 + 6H_2O \rightarrow 4NH_3 + 6CHO \quad \text{(i)}$$

$$NH_3 + H_2O \leftrightarrow NH_4^+ + OH^- \quad \text{(ii)}$$

$$Zn^{2+} + 2OH^- \rightarrow Zn(OH)_2 \quad \text{(iii)}$$

$$Zn(OH)_2 + 2OH^- \leftrightarrow Zn(OH)_4 \quad \text{(iv)}$$

$$Zn(OH)_4 \rightarrow ZnO + H_2O + 2OH^- \quad \text{(v)}$$

The ZnO nuclei are generated an undergo agglomeration to form particles. These ZnO nanoparticles get crystallized into hexagonal discs after gaining sufficient energy from the hydrothermal reaction conditions. Thus, the ZnO hexagonal nanodiscs generated by the aggregation and self-assembly of Zn nuclei presumably act as the growth units of ZnO. The ZnO nanorod structures are resulted from the stacking of ZnO hexagonal nanodiscs in a preferential orientation along the $(10\bar{1}0)$ and $(01\bar{1}0)$ crystallographic directions [27,28]. Furthermore, the MWCNTs were incorporated into the hydrothermal reaction which resulted into porous 3D hierarchical honeycomb ZnO structures. The normal growth habit of ZnO was inhibited due to the addition of MWCNTs, indicating that the MWCNTs might act as a structure-directing agent. This result is consistent with the previous reports [20,21]. It is proclaimed that the prior acid treatment to the MWCNTs introduces several active functional groups like −OH, −C═O, −C−O, and COOH which induces strong interaction among metal oxide particles and generally resulting into a structure with high porosity and large surface area [21,29]. Functionalized MWCNTs provides an orientation for ZnO nanosheets formation. These as formed sheet-like subunits further undergo interconnection during hydrothermal reaction conditions and resulting into formation of porous 3D hierarchical honeycomb structure. The different amounts of MWCNTs precursor solutions (5, 10, 15 ml) were introduced into the hydrothermal reaction to study their effect on surface morphology. There was no any significant change on the surface morphology observed, however the better 3D hierarchical ZnO honeycomb structures were found with addition of 10 ml MWCNTs precursor solution. Therefore, the further sample preparation and characterizations were performed with addition of only one concentration of MWCNTs precursor solution (10 ml). It is also important to note that not much incorporation of MWCNTs was observed as confirmed with FE-SEM and Raman analysis (Fig. 1c and d and Supporting information Fig. S2). The MWCNTs might be embedded into the ZnO structures or gone out with the residual powder solution. In order to incorporate MWCNTs an additional attempt was made using "dip and dry" method. Fig. 1e and f displays the FESEM micrographs of GZ2-2T photoelectrode, confirming incorporated MWCNTs into 3D hierarchical GaN/ZnO heterostructures.

Further to determine the phase, sizes and crystal structure of heterostructure FE-TEM analysis was acquired. A focused ion beam (FIB) technique was used to prepare the FE-TEM sample on a Cu grid (Supporting information Fig. S3). FE-TEM analysis showed different phases of counterparts with clear interfaces indicating heterostructure formation (Fig. 2a). The presence of the voids in the structure confirms the porous nature of the ZnO nanoflakes and embedded MWCNTs in agreement with the FE-SEM results. Fig. 2b represents a high-resolution TEM (HR-TEM) image of the GaN/ZnO interface. These results illustrate two distinct sets of lattice fringes with inter-planer distances of 0.33 and 0.26 nm, corresponding to the unstrained GaN and ZnO nanoflakes, respectively [12,30]. Similarly, a selected-area electron diffraction (SAED) pattern (Fig. 2c) shows bright spots in the line pattern due to the single-crystalline behavior of GaN crystals, which is correspond well with the (002) crystallographic plane. However, the ZnO nanoflakes (Fig. 2d) are represented by the ring line pattern, indicating the polycrystalline behavior of the ZnO nanoflakes, which corresponds well with the (100), (002), and (110) crystallographic planes. A layered energy-dispersive X-ray diffraction spectroscopy (EDS) mapping was also performed, which unambiguously represents the presence of all

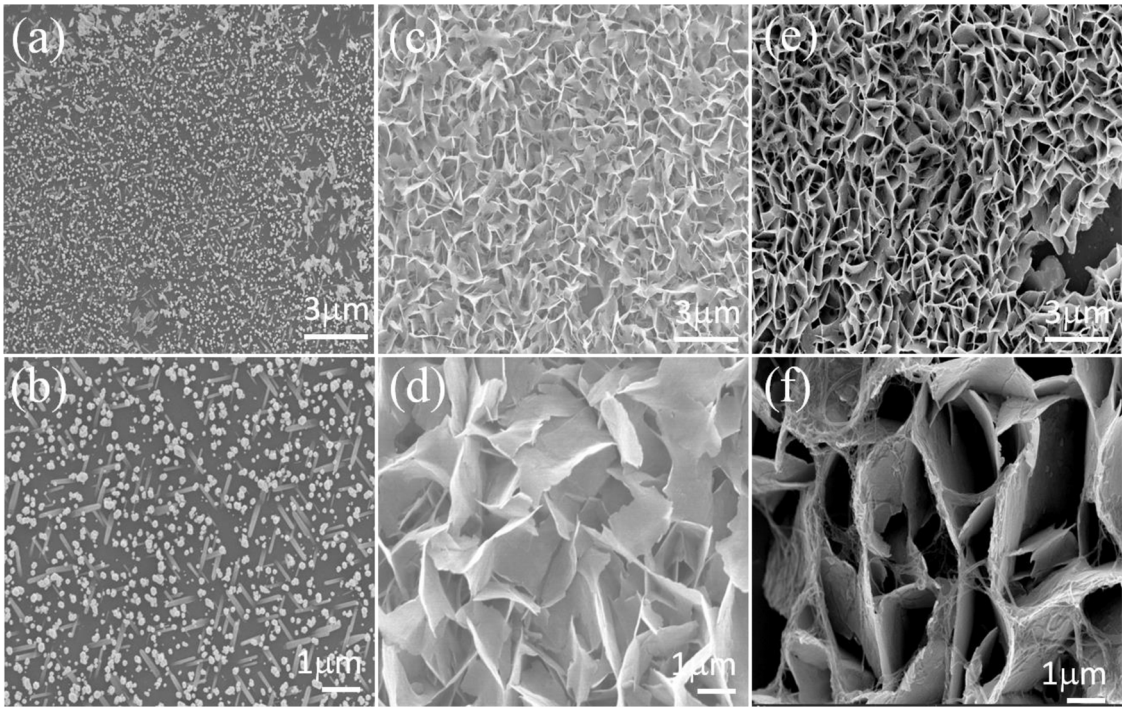

Fig. 1. FE-SEM micrographs of (a, b) GZ1, (c, d) GZ2, and (e, f) GZ2-2T samples.

three component phases in the sample (Supporting information Fig. S4 and Table S1). The right side of Fig. 2 shows the EDS elemental mapping of the sample, confirming the presence of the elements Zn, O, N, C, and Ga.

The phase of GaN/ZnO heterostructure photoelectrodes is determined by X-ray diffraction (XRD). Fig. 3a depicts the XRD pattern of GZ2-2T thin film which confirm the formation of ZnO with hexagonal phase (space group: P63mc) and calculated lattice constant values of a = 3.24 Å, b = 3.24 Å, and c = 5.20 Å (JCPDS card no. 05-0664). It is noted that no peaks corresponding to MWCNTs and GaN were observed, owing to the weak diffraction intensities of MWCNTs

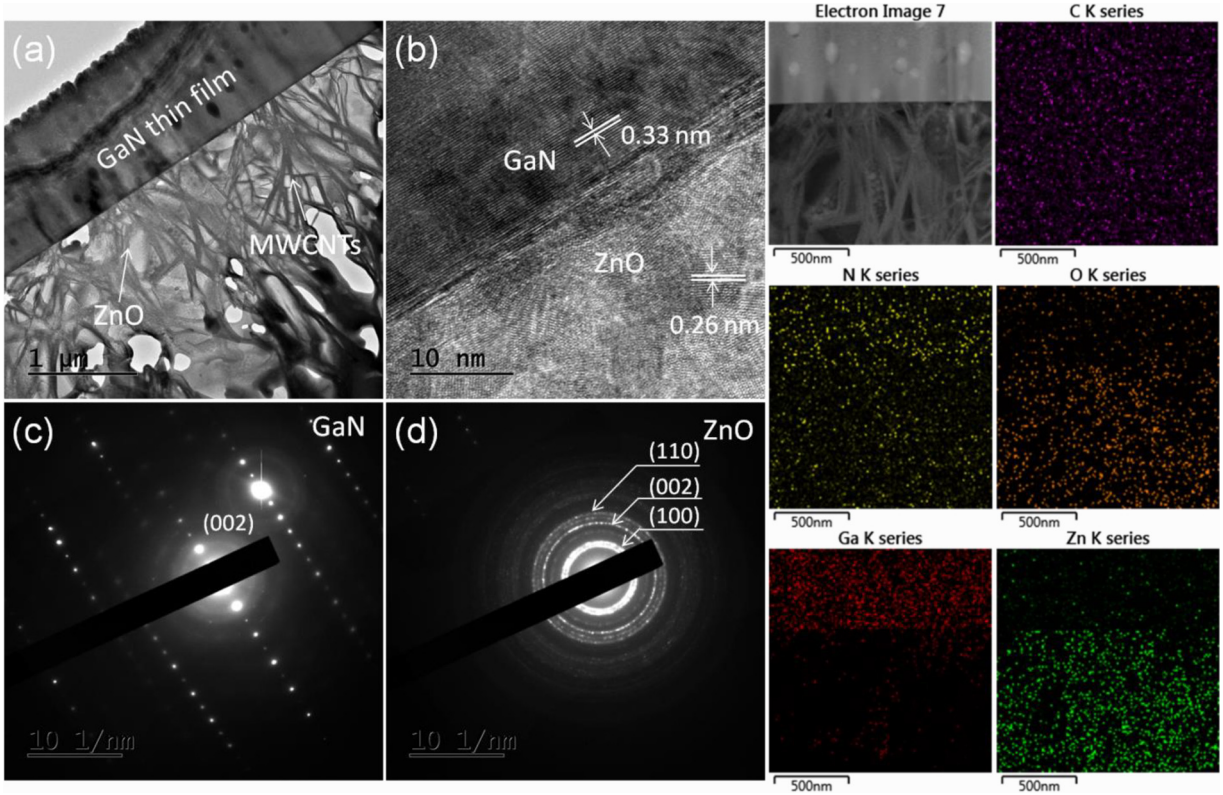

Fig. 2. FE-TEM images of GZ2-2T sample: (a, b) TEM and HRTEM image, (c) SAED pattern of GaN, and (d) SAED pattern of ZnO. The right side inset shows EDS elemental mapping.

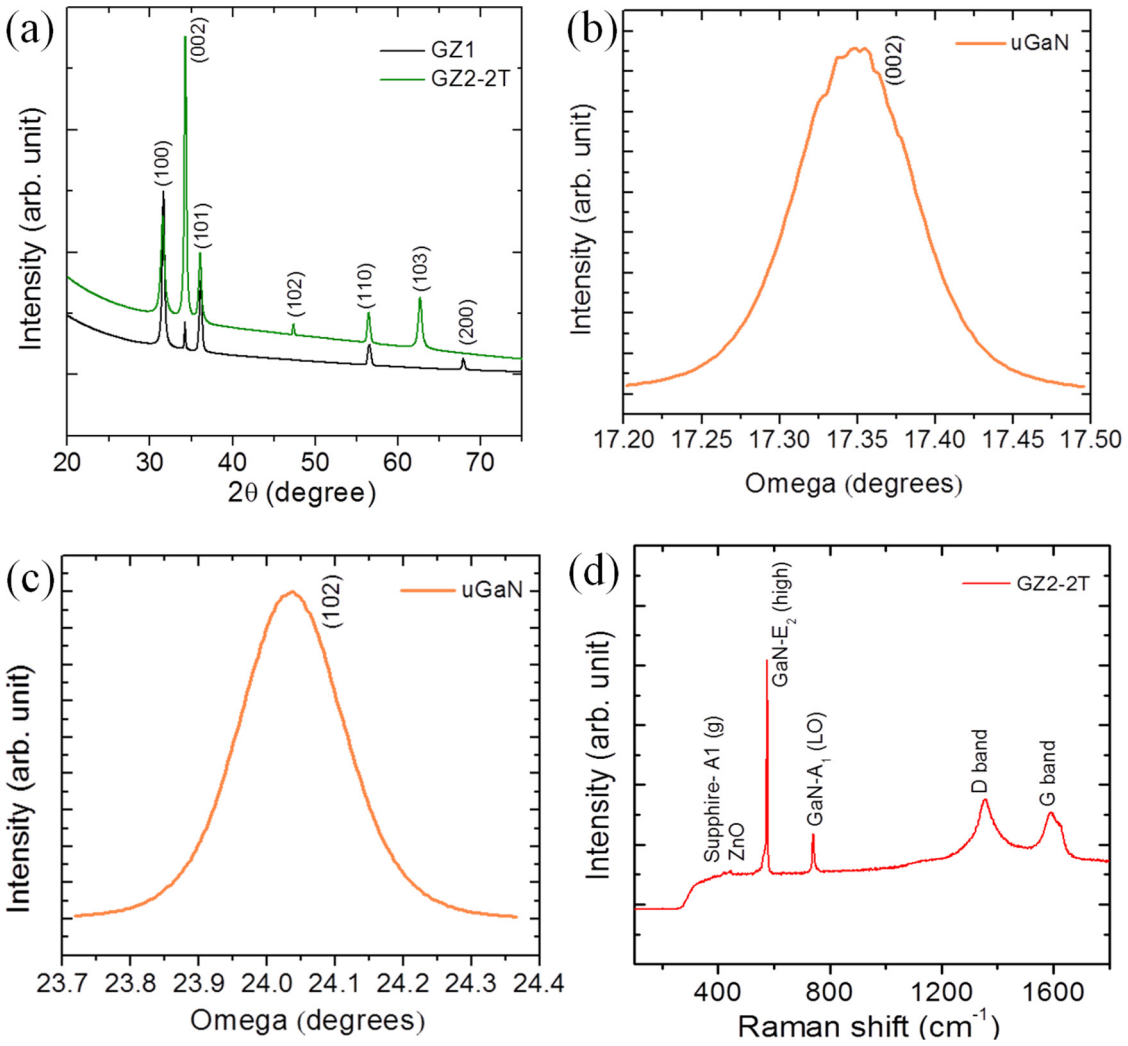

Fig. 3. XRD pattern of GZ1 and GZ2-2T hybrid heterostructures samples **(a)** Omega scan X-ray rocking curves of uGaN thin film sample: (b) (002) diffraction and (c) (102) diffraction. Raman spectrum of GZ2-2T hybrid heterostructures.

and GaN. The omega scan XRD was recorded to confirm the phase of the GaN, showing characteristic peaks at 17° and 24°, which indicate high crystal quality (Fig. 3b and c). The photoelectrodes were further examined by Raman spectroscopy, which showed multiple peaks corresponding to different emission modes (Fig. 3d). The peaks located at 569.8 and 735 cm^{-1} correspond to GaN and are attributed to the E_2 (high) and A_1 (low) phonon active modes, respectively [31]. Interestingly, the band at ~437 cm^{-1} was ascribed to the nonpolar optical phonon modes (high E2) from the ZnO emission [32]. In addition to this, the sapphire substrate exhibited Raman bands at around 419 cm^{-1} due to the A_{1g} phonon mode [32]. In the case of the GZ2-2T sample, additional Raman bands at around 1355 and 1590 cm^{-1} were observed, which correspond to the characteristic D and G bands of the integrated MWCNTs, respectively.

The surface elemental states of GZ2-2T photoelectrode was studied with X-ray photoelectron spectroscopy (XPS). Fig. 4a depicts the XPS survey spectrum showing presence of C, N, O, Ga and Zn in hybrid heterostructure. In Fig. 4b, the spin–orbit constituent of Ga2p (Fig. 3b) was deconvoluted into two peaks with binding energies of 1117.7 and 1144.6 eV, corresponding to the $Ga2p_{3/2}$ and $Ga2p_{1/2}$ states, respectively [33]. The binding energy difference of 26.9 eV between these two peaks represents the +3 oxidation state of gallium (Ga^{3+}) [33]. The deconvoluted N1s spectrum (Fig. 4c) showed a peak at 397.18 eV, indicating a Ga—N bond, whereas the peak at 399.6 eV could be attributed to the Ga—N—O species, in agreement with previous reports [34]. The XPS spectrum of Zn (Fig. 4d) presents peaks at binding energies of 1044.3 and 1021.1 eV, which are attributed to the $Zn2p_{5/2}$ and $Zn2p_{3/2}$ states, respectively, exhibiting a difference of 23.2 eV between the doublets and indicating presence of the Zn^{2+} state [30]. An asymmetric XPS spectrum was obtained for O1s (Fig. 4e), which indeed indicates the presence of various oxygen species ascribed to the lattice oxygen of ZnO (529.9 eV) and the surface hydroxyl species (531.6 eV) [30,35]. The C1s XPS spectrum of the MWCNTs (Fig. 4f) was deconvoluted into three peaks. The peak at 284.5 eV was attributed to the characteristic graphitic sp^2 carbon atoms and the other two peaks at 286.6 and 288.9 eV indicated the presence of epoxy/C—O, hydroxyl, and carbonyl (C═O) groups on the surface of the MWCNTs [36,37].

In order to identify the impact of coupling GaN photoanode with ZnO and MWCNTs, the linear sweep voltamograms (LSV) were recorded (Fig. 5a). Negligible dark currents were found for all prepared photoanodes, whereas the current density was dramatically enhanced under the light illumination indicating good photoactive behavior. The photocurrents were generated at approximately −0.45 V applied bias (V_{onset}), which further increased linearly and then saturates beyond 0.8 V. The pristine GaN photoanode exhibited a noticeable photocurrent density (J_{ph}) of 1.14 mA/cm^2 at zero bias. In comparison to bare GaN, all the heterostructure GaN/ZnO photoanodes exhibited better improvement in the PEC performance. The GaN/ZnO heterostructure photoanode (GZ1) with mixed rod/disc-like morphological structures has showed a J_{ph} value of 1.70 mA/cm^2, which represents a 1.49-fold

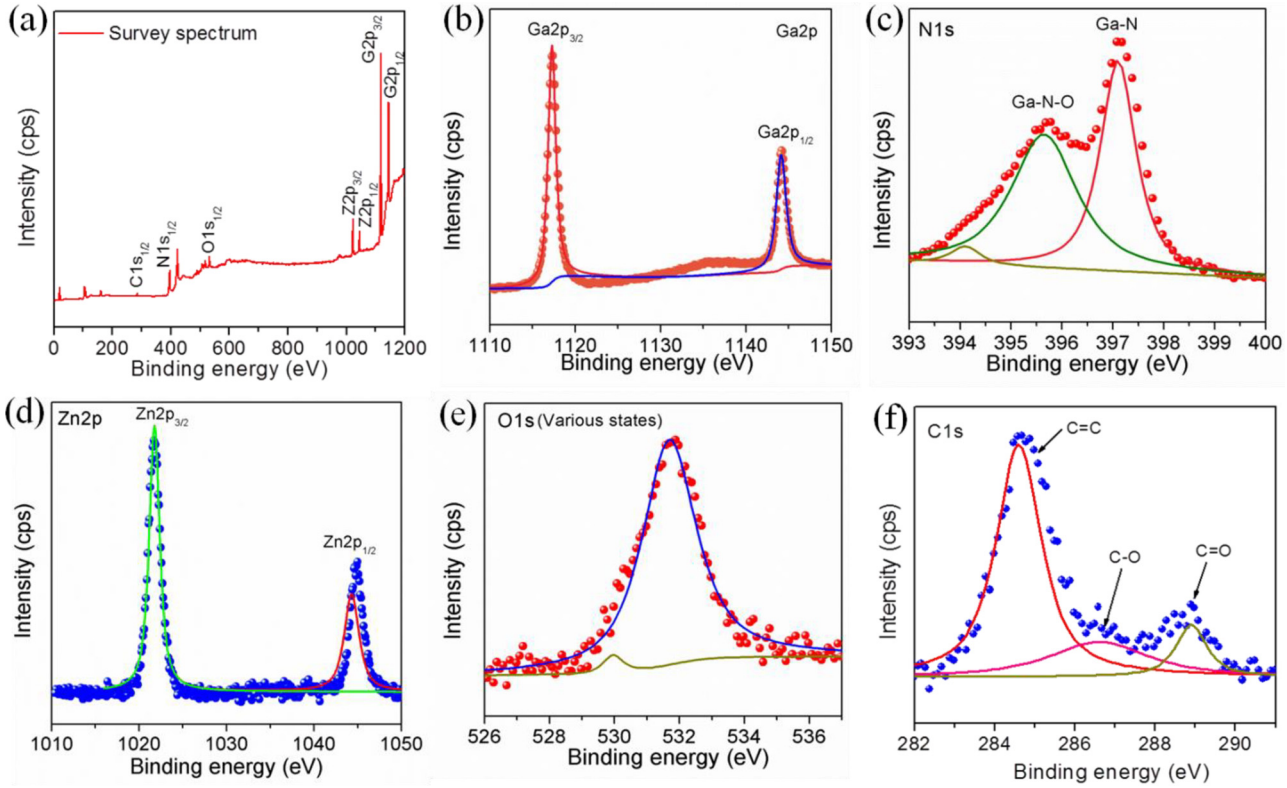

Fig. 4. XPS spectra of GZ2-2T sample: (a) survey spectrum, (b) Ga2p, (C) N1s, (d) Zn2p, (e) O1s, and (f) C1s.

increase compared to that of bare GaN (1.14 mA/cm^2). Interestingly, the J_{ph} value was significantly improved for the MWCNT-assisted in-situ prepared GaN/ZnO heterostructure electrodes (GZ2) (2.78 mA/cm^2), which might be due to the special porous ZnO nanoflake structures that cover all the surface area of the GaN, making good interfacial contact and offering more surface active sites for the PEC reactions. It should be noted that the additional deposition of MWCNTs on GaN/ZnO heterostructures (GZ2-2T) by a dip-and-dry method showed an even better improvement in the J_{ph} value (3.02 mA/cm^2). Thus, the highest J_{ph} of 2.78 and 3.02 mA/cm^2 were achieved at zero bias for the heterostructure GZ2 and GZ2-2T photoelectrodes, respectively, which are approximately 2.37 and 2.58 times higher than that of the pure GaN photoelectrode. To the best of our knowledge, these are the highest values achieved for GaN:ZnO photoanodes (Table S3). For fair comparison, the dip and dry coating method for excessive deposition of MWCNTs was employed on GZ1 (GZ1-2T) which revealed improvement in the photocurrent density of 2.58 mA/cm^2, approximately 1.51 times higher than GZ1 (Supporting information Fig. S7). It is also noteworthy that the bare MWCNTs exhibit very low PEC performance (Supporting information Fig. S7). Similarly, there is no obvious difference in the PEC performance of GZ2 and GZ2-2T, indicating that the less effect of the excessively deposited MWCNTs. Therefore, the improved PEC performance of GZ2-2T photoanode might be due to the formation of much more porous ZnO structures which has good mechanical strength, more active sites and open spaces between the nanosheets which indeed help for enhancing dissipation of generated gaseous products [38]. The UV–vis absorption spectra were recorded to evaluate the optical properties of the as prepared photoanodes (Fig. S8). The pristine GaN electrode showed light absorption around 365 nm which is slightly shifted to the higher wavelengths with incorporation of both MWCNTs and ZnO heterostructure indicating smaller increase in the absorption capability (379 nm for GZ2-2T).

To gain more insights into the enhanced PEC-WS performance of the ternary heterostructure GZ2-2 T photoanode, the incident photon-to-current efficiency (IPCE) was determined using monochromatic light irradiation. The IPCE was calculated at an applied bias of 0.5 V,

$$IPCE(\%) = \frac{1240(V \times nm) \times J_{ph}(mA/cm^2)}{\lambda(nm) \times P_{light}(mW/cm^2)} \times 100, \quad (1)$$

where λ is the wavelength of the monochromatic photons, the factor 1240 represents the product of the speed of light and Planck's constant, and P_{light} is the power density of the light at a given wavelength. The highest IPCE of 14.2% was obtained for the GZ2-2T photoanode at 350 nm, which is higher than those of the GZ1 (11.9%), GZ2 (12.8%), and bare GaN (10.1%) photoelectrodes (Fig. 5b). To further elucidate high PEC efficiency of the GaN/ZnO/MWCNTs hybrid photoanodes, the applied bias photon-to-current efficiency (ABPE) was determined by

$$ABPE(\%) = \frac{J_{ph}(mA/cm^2) \times (1.23 - |V_{app}|)(V)}{P_{light}(mW/cm^2)} \times 100, \quad (2)$$

where $|V_{app}|$ is the applied bias during the measurement of the J_{ph}. Here, J_{ph} is the measured photocurrent density, 1.23 V is the standard state reversible potential of water, and P_{light} is the power density of illuminating light source. The improved ABPE value of ~0.95% was estimated for the GZ2-2T photoelectrode, which is approximately 2.06 times higher than that of a pristine GaN photoelectrode sample (0.46%) (Fig. 5c). The as-obtained J_{ph} and ABPE values are significantly higher than those of recently reported GaN and GaN/InGaN, GaN/ZnO photoanodes [12,19,39]. To better understand the enhanced PEC performance of the ternary GaN/ZnO/MWCNTs photoanode, we performed an electrochemical impedance spectroscopy (EIS) analysis under dark conditions in the frequency range of 1 MHz – 1 Hz at an amplitude of 10 mV. Fig. 5d depicts the Nyquist plots fitted according to the equivalent circuit model, where R_s represents the solution resistance, R_{ct} is the interface charge transport resistance, W is the Warburg impedance, and Q represents the constant phase element (CPE). Generally, the diameters of the semicircle in the Nyquist plots are considered to evaluate the charge transfer characteristics of photoelectrodes. The semicircle diameters are directly proportional to the charge transfer

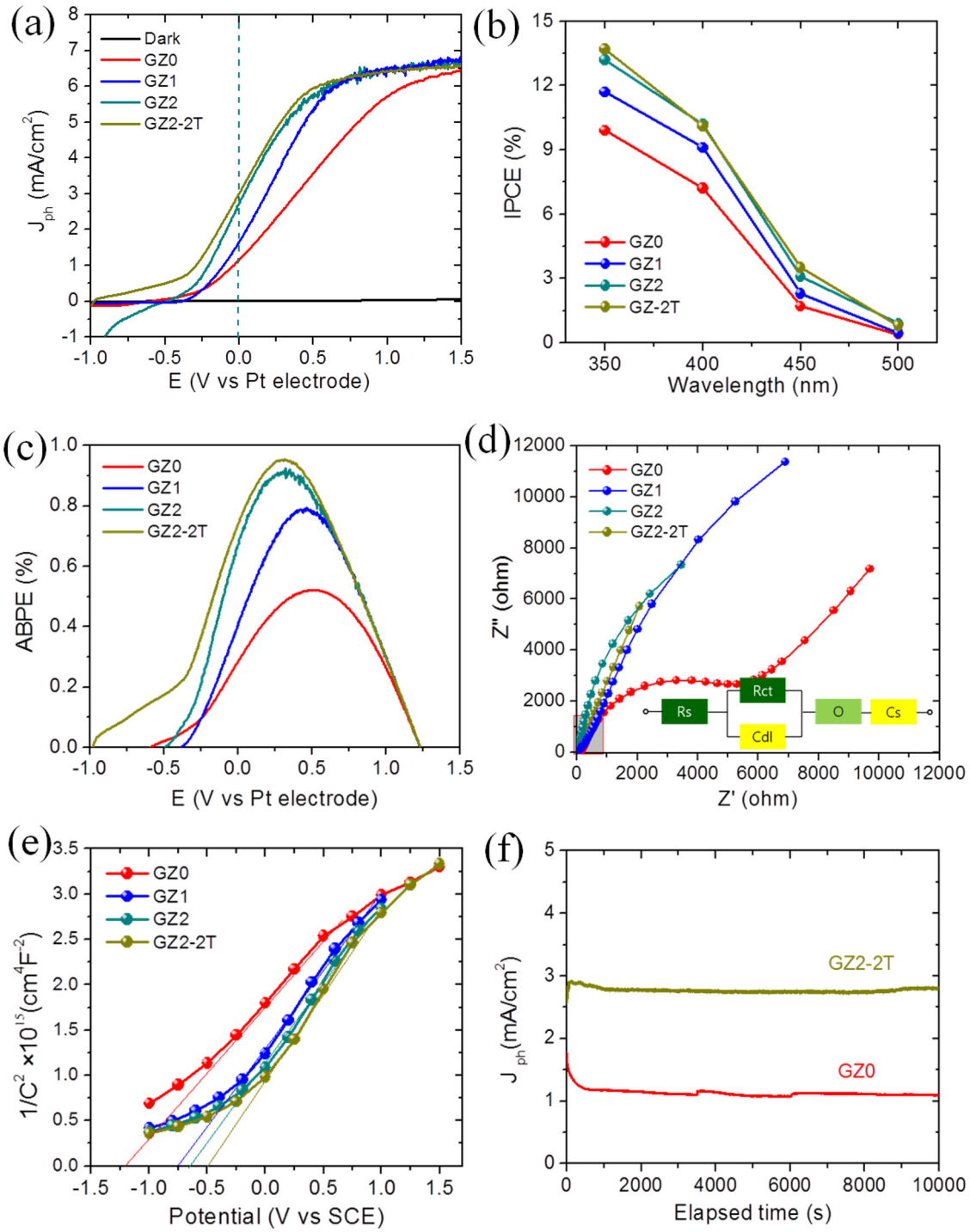

Fig. 5. Photoelectrochemical characterization of as fabricated GZ0, GZ1, GZ2, and GZ3-2T photoelctrodes (a) Linear sweep voltametry (LSV) curves in 0.5 M NaOH electrolyte (b) incident photon-to-current conversion efficiency (c) applied-bias-to-photon conversion efficiency (ABPE%) (d) Nyquist plots; Inset shows the equivalent circuit diagram (e) Mott-Schottky plots. and (f) Chronoamperimetric J–T curves.

resistances at the semiconductor–electrolyte interfaces. The charge-transfer resistance (R_{ct}) values were found to be 22219, 20564, 18826, and 3802 Ω/cm^2 for the GZ0, GZ1, GZ2, and GZ2-2T photoelectrodes respectively. The lowest values of R_{ct} for the photoanode GZ2-2T clearly indicates faster charge transportation within composite heterostructure photoanodes. The solution resistance values (R_s) were also obtained which were found to be 97.02, 7.42, 6.14, 4.93 Ω/cm^2 for the photoanodes GZ0, GZ1, GZ2, and GZ2-2T, respectively. The lowered resistance values represent better conductivity of heterostructure photoanode due to MWCNTs modification. Fig. 5e displays the Mott-Schottky plot which is commonly used to determine the flat band potential of photoelectrodes. The flat band potentials (V_{fb}) can be calculated from x-axis intercept using Eq. (3)

$$\frac{1}{C2} = \left(\frac{2}{e_0 \varepsilon \varepsilon_0 N_d}\right)\left[(V - V_{FB}) - \frac{kT}{e_0}\right] \quad (3)$$

Where e_0 is fundamental charge constant, ε and ε_o are the dielectric constant and vacuum permittivity of semiconductor, N_d is the charge carrier density, C is the space charge capacitance in the semiconductor, V is the applied potential, V_{FB} is the flat band potential, T is the

temperature, and k is the Boltzmann constant. In theory, the flat band potential values are equal to the onset potential of measured photocurrent therefore suggesting as an important PEC characterization tool [23]. The flat band potential values were observed to be −1.24 V and −0.51 V for GZ0 and GZ2-2T photoanodes. The flat band potential is shifted to more positive values due to MWCNTs hybridization which are consistent with the previous reports [23,40]. Thus, the enhanced PEC performance can be attributed to the constructive effect of heterostructure offering better conductivity, and rapid access for the interfacial charge transfer. The electrochemical active surface area (ECSA) was calculated to confirm the enhanced PEC activity of the GZ2-2T electrode (Supporting information S9). It is well-known that an increase in the ECSA accelerates the catalytic activity of the electrode [38,41]. The ECSA is proportional to the electrochemical double layer capacitance, C_{dl} [38]. C_{dl} was calculated from the cyclic voltametry (CV) curves. The C_{dl} and corresponding ECSA values of the studied catalysts are summarized in Table S3. The large C_{dl} (0.212 μF/cm^2) and thereby higher ECSA (0.0052 cm^2) of GZ2-2T electrode indicates that higher electrochemical active surfaces of electrode are in contact with electrolyte which enhances the water oxidation catalytic activity.

GaN photoelectrodes are generally succumbed to photocorrosion problem; therefore, it is crucial to evaluate the long term stability of as prepared ternary heterostructure photoelectrodes. Choronoamperometric *J–T* curves are recorded over the period of 10,000 s for GZ0 and GZ2-2T photoanodes (Fig. 5f). It can be seen that the ternary heterostructure (GZ2-2T) shows an enhanced stability with photocurrent retention of ~2.87 mA/cm^2. In contrast, the *J–T* curves of pristine GaN (GZ0) photoanode showed low photocurrent density retention (~1.08 mA/cm^2) and periodic fluctuations in the photocurrent. MWCNTs alone does not give significant PEC performance, however their combined effect with other semiconductors in the form of hybrids can provide better PEC water oxidation stability due to their structural integrity and chemical inertness [42].

To better understand PEC-WS process, a schematic representation of photoelectrochemical mechanism is illustrated (Fig. 6). It should be noted that GaN/ZnO heterojunction forms a type-II band alignment, which can facilitate the separation of photogenrated charge carriers (e^-/h^+) across interface [6,18]. Here, MWCNTs are incorporated with wide band gap GaN/ZnO semiconductor heterojunction which help composite photoanode to exhibit visible light photoactivity [43]. This is due to the fact that the MWCNTs could act as photosensitizer instead of mere adsorbent and dispersing reagent [20]. On the basis of previous reports and our present results we believe that the strong interfacial interaction between MWCNTs and GaN/ZnO infers photosensitizer-induced visible light photoactivity towards PEC water splitting. Under visible light illumination, MWCNTs in the GaN/ZnO/MWCNTs composite heterostructure is photoexcited from the ground-state MWCNTs to the excited-state MWCNTs* which generates photo-generated electrons [44,45]. The MWCNTs* in the excited state then injects electrons into the conduction band of ZnO and subsequently migrated to the conduction band of GaN [43,46]. The electrons would finally transfer to the Pt counter electrode, wherein they are utilized for water reduction to trigger the evolution of hydrogen (H_2). Meanwhile, photo-induced holes would move from the valence band of GaN to the valence band of ZnO, wherein utilized for the water oxidation producing O_2. Such a similar photocatalytic systems and reaction mechanisms has been proposed in the past with different photosensitizers including C60, graphene, MWCNTs. For instance, Kamat et al. [47] have reported that for the C60/TiO_2 composite photocatalyst, C60 can be photo-excited under visible light laser beam irradiation, and the photogenereated electrons in C60 can be transferred to the conduction band of TiO_2. Yang et al. [45] have proposed three basic precondition requirements to experimentally observe the exact photosensitizer role of graphene (similar to MWCNTs) in the graphene-ZnO composites (i) for the graphene–semiconductor composites under visible light irradiation, the semiconductor by itself should be unable to be band gap-photoexcited; (ii) the proper interfacial interaction between graphene and the semiconductor should be needed to achieve the better charge carrier lifetime and transfer efficiency (iii) the suitable probe reactions should be chosen to avoid the self-induced photosensitization effect (e.g., organic dye photosensitization for semiconductor). Wang et al. [43] have reported that CNT might act as photosensitizer for TiO_2 under visible light irradiation, which could transfers the photo-induced electrons from the CNT to the CB of TiO_2/CNT photocatalyst. This suggests that the MWCNTs in GaN/ZnO/MWCNTs heterostructure allow photosensitizer induced charge excitation whereas the intimate interfacial interaction between GaN and ZnO is beneficial for reducing unwanted recombination of e^-/h^+ pairs. This is further confirmed by evaluating the photoanodes using photoluminescence (PL) study since, it is known to give insights into charge carrier separation efficiency. PL emission is mainly resulted from the recombination of excited e^-/h^+ and the reduction in PL intensity indicates reduced charge carrier recombination efficiency [48].

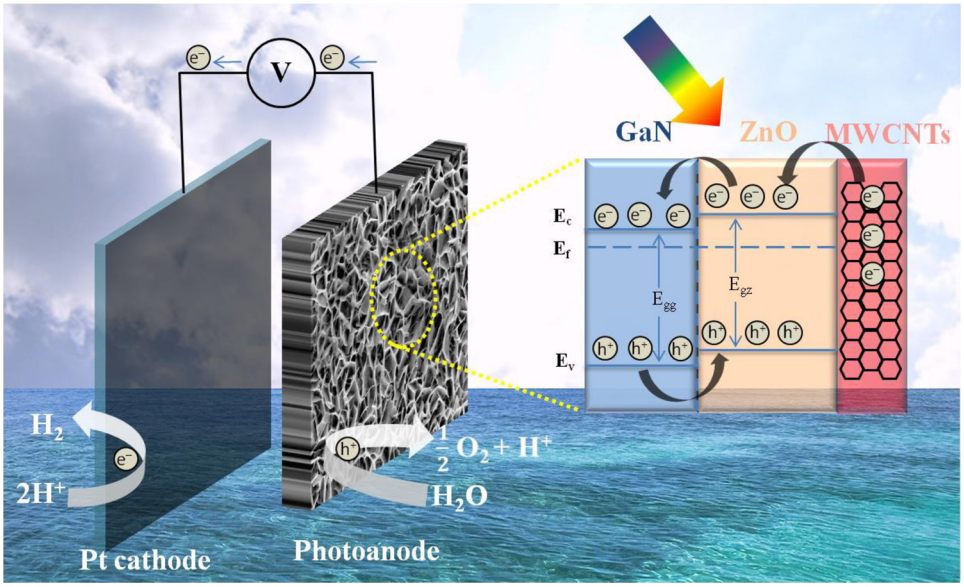

Fig. 6. Schematic representation of PEC water splitting mechanism for ternary heterostructure GaN/ZnO/MWCNTs. E_{gg} is the bandgap of GaN, E_{gz} is the bandgap of ZnO, E_f is the Fermi level, E_v and E_c represents the valence band and conduction band levels, respectively.

As seen from Fig. S10, the PL intensity of GZ2-2T electrode was drastically reduced with incorporation of ZnO and MWCNTs. This might be due interfacial band bending which help to improve the charge carrier separation efficiency and PEC performance [4,48]. Overall, the enhanced PEC performance of heterostructure photoanodes could be attributable to (a) the formation of the GaN/ZnO heterostructure, which promotes the effective separation of photo-excited electrons and holes leading to extending their lifetime; (b) the unique, porous 3D hierarchical nanostructures providing high electrode/electrolyte contact area as well as voids to transfer light to the underlying GaN thin film; (c) the hybridized MWCNTs which not only tune the surface texture but also provide channels for visible light sensitization and electron transportation.

4. Conclusion

In summary, we explore the heterojunction construction strategy to improve PEC water oxidation performance of GaN photoanode. The new approach involved in-situ growth of heterostructured photoanodes which removes an intermediate stage of using preformed semiconductor particles. We investigated the role of MWCNTs in tuning porous 3D honeycomb ZnO/GaN heterostructures. The as fabricated heterostructure is composed of self assembly of porous ZnO thin nanosheets and MWCNTs. Moreover, fabricating ZnO porous nanostructures on underlying GaN is beneficial for trapping light through their voids which in turn help to improve the photocurrent density. The hierarchical ternary heterostructure GaN/ZnO/MWCNTs photoanode promises unassisted PEC water splitting with enhanced photocurrent density of 3.02 mA/cm^2 under 1-sun light illumination, which is a ~2.58 time higher than that of pristine GaN photoelectrode having photocurrent of 1.14 mA/cm^2. The ternary heterostructure GaN/ZnO/MWCNTs photoanode also achieves higher values of IPCE (~14.2%) and ABPE (~0.95%) at wavelength 350 nm and applied bias 0.5 V, respectively. Similarly, GaN/ZnO/MWCNTs photoanode shows higher value of ECSA (0.0052 cm^2) which indicates the higher electrochemical active surfaces are in contact with electrolyte which enhances water oxidation catalytic activity. The synergy of physicochemical synthesis highlights a useful approach for fabricating hierarchical functional materials which can pave the ways for solar energy conversion devices.

Acknowledgement

This work was supported by the National Research Foundation of Korea Grant funded by the Korean Government (NRF-2016R1A2B4008622).

Appendix A. Supplementary data

Supplementary material related to this article can be found, in the online version, at doi:https://doi.org/10.1016/j.apcatb.2018.06.047.

References

[1] A. Landman, H. Dotan, G.E. Shter, M. Wullenkord, A. Houaijia, A. Maljusch, et al., Photoelectrochemical water splitting in separate oxygen and hydrogen cells, Nat. Mater. 16 (2017) 646.
[2] T. Hisatomi, J. Kubota, K. Domen, Recent advances in semiconductors for photocatalytic and photoelectrochemical water splitting, Chem. Soc. Rev. 43 (2014) 7520–7535.
[3] K. Sivula, R. Van De Krol, Semiconducting materials for photoelectrochemical energy conversion, Nat. Rev. Mater. 1 (2016).
[4] S.S. Patil, M.G. Mali, M.A. Hassan, D.R. Patil, S.S. Kolekar, S.-W. Ryu, One-pot in situ hydrothermal growth of BiVO4/Ag/rGO hybrid architectures for solar water splitting and environmental remediation, Sci. Rep. 7 (2017) 8404.
[5] J. Sun, D.K. Zhong, D.R. Gamelin, Composite photoanodes for photoelectrochemical solar water splitting, Energy Environ. Sci. 3 (2010) 1252–1261.
[6] H. Zhang, D. Wu, Q. Tang, L. Liu, Z. Zhou, ZnO-GaN heterostructured nanosheets for solar energy harvesting: computational studies based on hybrid density functional theory, J. Mater. Chem. A 1 (2013) 2231–2237.
[7] K. Wysmulek, J. Sar, P. Osewski, K. Orlinski, K. Kolodziejak, A. Trenczek-Zajac, et al., A SrTiO3-TiO2 eutectic composite as a stable photoanode material for photoelectrochemical hydrogen production, Appl. Catal. B Environ. 206 (2017) 538–546.
[8] S.S. Patil, D.R. Patil, S.K. Apte, M.V. Kulkarni, J.D. Ambekar, C.-J. Park, et al., Confinement of Ag_3PO_4 nanoparticles supported by surface plasmon resonance of Ag in glass: efficient nanoscale photocatalyst for solar H_2 production from waste H_2S, Appl. Catal. B Environ. 190 (2016) 75–84.
[9] J. Resasco, H. Zhang, N. Kornienko, N. Becknell, H. Lee, J. Guo, et al., TiO2/$BiVO_4$ nanowire heterostructure photoanodes based on type II band alignment, ACS Cent. Sci. 2 (2016) 80–88.
[10] H. Yu, X. Quan, S. Chen, H. Zhao, TiO_2−multiwalled carbon nanotube heterojunction arrays and their charge separation capability, J. Phys. Chem. C 111 (2007) 12987–12991.
[11] H. Bai, J. Juay, Z. Liu, X. Song, S.S. Lee, D.D. Sun, Hierarchical $SrTiO_3$/TiO_2 nanofibers heterostructures with high efficiency in photocatalytic H_2 generation, Appl. Catal. B Environ. 125 (2012) 367–374.
[12] M. Ebaid, J.-H. Kang, S.-H. Lim, J.-S. Ha, J.K. Lee, Y.-H. Cho, et al., Enhanced solar hydrogen generation of high density, high aspect ratio, coaxial InGaN/GaN multi-quantum well nanowires, Nano Energy 12 (2015) 215–223.
[13] X.-L. Yin, L.-L. Li, W.-J. Jiang, Y. Zhang, X. Zhang, L.-J. Wan, et al., MoS_2/CdS nanosheets-on-nanorod heterostructure for highly efficient photocatalytic H2 generation under visible light irradiation, ACS Appl. Mater. Interfaces 8 (2016) 15258–15266.
[14] X. Zhang, Y. Yang, S. Ding, W. Que, Z. Zheng, Y. Du, Construction of high-quality SnO_2@MoS_2 nanohybrids for promising photoelectrocatalytic applications, Inorg. Chem. 56 (2017) 3386–3393.
[15] L. Zhu, M. Hong, G. Wei Ho, Hierarchical assembly of SnO_2/ZnO nanostructures for enhanced photocatalytic performance, Sci. Rep. 5 (2015) 11609.
[16] Y. Hou, F. Zuo, A. Dagg, P. Feng, Visible light-driven α-Fe_2O_3 nanorod/graphene/$BiV_{1-x}Mo_xO_4$ core/shell heterojunction array for efficient photoelectrochemical water splitting, Nano Lett. 12 (2012) 6464–6473.
[17] A. Kargar, Y. Jing, S.J. Kim, C.T. Riley, X. Pan, D. Wang, ZnO/CuO heterojunction branched nanowires for photoelectrochemical hydrogen generation, ACS Nano 7 (2013) 11112–11120.
[18] H. Pan, Y.-W. Zhang, GaN/ZnO superlattice nanowires as photocatalyst for hydrogen generation: a first-principles study on electronic and magnetic properties, Nano Energy 1 (2012) 488–493.
[19] Z. Wang, J. Han, Z. Li, M. Li, H. Wang, X. Zong, et al., Moisture-assisted preparation of compact GaN:ZnO photoanode toward efficient photoelectrochemical Water oxidation, Adv. Energy Mater. 6 (2016) 1600864–n/a..
[20] W.-D. Zhang, B. Xu, L.-C. Jiang, Functional hybrid materials based on carbon nanotubes and metal oxides, J. Mater. Chem. 20 (2010) 6383–6391.
[21] W. Li, P. Wu, S. Yang, Y. Zhu, C. Kang, L.T. Tran, et al., 3D hierarchical honeycomb structured MWCNTs coupled with CoMnAl-LDO: fabrication and application for ultrafast catalytic degradation of bisphenol A, RSC Adv. 5 (2015) 8859–8867.
[22] A. Jitianu, T. Cacciaguerra, R. Benoit, S. Delpeux, F. Béguin, S. Bonnamy, Synthesis and characterization of carbon nanotubes–TiO_2 nanocomposites, Carbon N. Y. 42 (2004) 1147–1151.
[23] J.Y. Kim, H. Jun, S.J. Hong, H.G. Kim, J.S. Lee, Charge transfer in iron oxide photoanode modified with carbon nanotubes for photoelectrochemical water oxidation: an electrochemical impedance study, Int. J. Hydrogen Energy 36 (2011) 9462–9468.
[24] D. Sengupta, B. Mondal, K. Mukherjee, Genesis of flake-like morphology and dye-sensitized solar cell performance of Al-doped ZnO particles: a study, J. Nanopart. Res. 19 (100) (2017).
[25] Y.V. Kaneti, J. Yue, X. Jiang, A. Yu, Controllable synthesis of ZnO nanoflakes with exposed (10$\bar{1}$0) for enhanced gas sensing performance, J. Phys. Chem. C 117 (2013) 13153–13162.
[26] G. Sun, H. Yang, C. Ma, Y. Zhang, J. Yu, W. He, et al., Application of CuS-functionalized ZnO nanoflakes for a paper-based photoelectrochemical immunoassay using an in situ electron donor producing strategy, New J. Chem. 39 (2015) 7012–7018.
[27] R. Boppella, K. Anjaneyulu, P. Basak, S.V. Manorama, Facile synthesis of face oriented ZnO crystals: tunable polar facets and shape induced enhanced photocatalytic performance, J. Phys. Chem. C 117 (2013) 4597–4605.
[28] A. Wei, X.W. Sun, C.X. Xu, Z.L. Dong, Y. Yang, S.T. Tan, W. Huang, Growth mechanism of tubular ZnO formed in aqueous solution, Nanotechnology 17 (2006) 1740.
[29] D. Benetti, K.T. Dembele, J. Benavides, H. Zhao, S. Cloutier, I. Concina, et al., Functionalized multi-wall carbon nanotubes/TiO_2 composites as efficient photoanodes for dye sensitized solar cells, J. Mater. Chem. C 4 (2016) 3555–3562.
[30] S.S. Patil, M.G. Mali, M.S. Tamboli, D.R. Patil, M.V. Kulkarni, H. Yoon, et al., Green approach for hierarchical nanostructured Ag-ZnO and their photocatalytic performance under sunlight, Catal. Today 260 (2016) 126–134.
[31] T.C. Shibin Krishna, N. Aggarwal, G.A. Reddy, P. Dugar, M. Mishra, L. Goswami, et al., Probing the correlation between structure, carrier dynamics and defect states of epitaxial GaN film on (1120) sapphire grown by rf-molecular beam epitaxy, RSC Adv. 5 (2015) 73261–73267.
[32] B. Viana, O. Lupan, T. Pauporté, Directional and magnetic field enhanced emission of Cu-doped ZnO nanowires/p-GaN heterojunction light-emitting diodes, J. Nanophoton. 5 (2011) 51816–51818.
[33] M. Ebaid, D. Priante, G. Liu, C. Zhao, M. Sharizal Alias, U. Buttner, et al., Unbiased photocatalytic hydrogen generation from pure water on stable Ir-treated In0.33Ga0.67N nanorods, Nano Energy 37 (2017) 158–167.
[34] S. Wang, L. Zhang, C. Sun, Y. Shao, Y. Wu, J. Lv, et al., Gallium nitride crystals:

novel supercapacitor electrode materials, Adv. Mater. 28 (2016) 3768–3776.
[35] S.S. Patil, D.P. Dubal, V.G. Deonikar, M.S. Tamboli, J.D. Ambekar, P. Gomez-Romero, et al., Fern-like rGO/$BiVO_4$ hybrid nanostructures for high-energy symmetric supercapacitor, ACS Appl. Mater. Interfaces 8 (2016) 31602–31610.
[36] W.-S. Tseng, C.-Y. Tseng, C.-T. Kuo, Effects of gas composition on highly efficient surface modification of multi-walled carbon nanotubes by cation treatment, Nanoscale Res. Lett. 4 (2008) 234.
[37] G.M. Thorat, H.S. Jadhav, W.-J. Chung, J.G. Seo, Collective use of deep eutectic solvent for one-pot synthesis of ternary Sn/SnO_2@C electrode for supercapacitor, J. Alloys Compd. 732 (2018) 694–704.
[38] B. Pravin, L. Abhishek, S.H. Ho, P. Bharati, G.M. Gil, P. Sambhaji, et al., Cobalt iron hydroxide as a precious metal-free bifunctional electrocatalyst for efficient overall Water splitting, Small 14 (2017) 1702568.
[39] C. Yang, L. Liu, S. Zhu, Z. Yu, X. Xi, S. Wu, et al., GaN with laterally aligned nanopores to enhance the water splitting, J. Phys. Chem. C 121 (2017) 7331–7336.
[40] D. Chaudhary, S. Singh, V.D. Vankar, N. Khare, A ternary Ag/TiO_2/CNT photoanode for efficient photoelectrochemical water splitting under visible light irradiation, Int. J. Hydrogen Energy 42 (2017) 7826–7835.
[41] C.C.L. McCrory, S. Jung, J.C. Peters, T.F. Jaramillo, Benchmarking heterogeneous electrocatalysts for the oxygen evolution reaction, J. Am. Chem. Soc. 135 (2013) 16977–16987.
[42] S. Rai, A. Ikram, S. Sahai, S. Dass, R. Shrivastav, V.R. Satsangi, CNT based photoelectrodes for PEC generation of hydrogen: a review, Int. J. Hydrogen Energy 42 (2017) 3994–4006.
[43] W. Wang, P. Serp, P. Kalck, J.L. Faria, Visible light photodegradation of phenol on MWNT-TiO_2 composite catalysts prepared by a modified sol–gel method, J. Mol. Catal. A Chem. 235 (2005) 194–199.
[44] W. Oh, M. Chen, Synthesis and characterization of CNT/TiO_2 composites thermally derived from MWCNT and titanium (IV) n-butoxide, Bull. Korean Chem. Soc. 29 (2008) 159–164.
[45] M.-Q. Yang, Y.-J. Xu, Basic principles for observing the photosensitizer role of graphene in the graphene–semiconductor composite photocatalyst from a case study on graphene–ZnO, J. Phys. Chem. C 117 (2013) 21724–21734.
[46] Y. Zhang, N. Zhang, Z.-R. Tang, Y.-J. Xu, Graphene transforms wide band gap ZnS to a visible light photocatalyst. The new role of graphene as a macromolecular photosensitizer, ACS Nano 6 (2012) 9777–9789.
[47] P.V. Kamat, M. Gevaert, K. Vinodgopal, Photochemistry on semiconductor surfaces. Visible light induced oxidation of C60 on TiO_2 nanoparticles, J. Phys. Chem. B 101 (1997) 4422–4427.
[48] A. Wang, Y. Wang, W. Yu, Z. Huang, Y. Fang, L. Long, et al., TiO_2-multi-walled carbon nanotube nanocomposites: hydrothermal synthesis and temporally-dependent optical properties, RSC Adv. 6 (2016) 20120–20127.